# Using Drive-by Health Monitoring to Detect Bridge Damage Considering Environmental and Operational Effects

William Locke[1,*], Justin Sybrandt[2], Ilya Safro[2], Sez Atamturktur[3]

*Clemson, SC. USA*

**Abstract**

Drive-by Health Monitoring utilizes accelerometers mounted on commercial and civilian vehicles to gather dynamic response data that can be used to continuously evaluate the health of bridges faster and with less equipment than traditional structural health monitoring practices. Because vehicles and bridges create a coupled system, vehicle acceleration data contains information about bridge frequencies that can be used as health indicators. However, for drive-by health monitoring to be viable, variabilities in dynamic measurements caused by environmental and operational parameters, such as temperature, vehicle speed, traffic, and surface roughness need to be considered. In this paper, a finite element model of a simply supported bridge is developed considering the aforementioned variabilities and various levels of structural damage. Vehicle acceleration data obtained from the model is then transformed to the frequency domain and processed using a multi-layer neural network. This method is used to determine the relationships between noise inducing variables and changes in vehicle dynamic response spectrum; these relationships are leveraged to predict the overall health of the subject bridge. The results from this study indicate that the developed methodology, drive-by health monitoring data analyzed with a multi-layer neural network, can serve as a viable health monitoring strategy and should be further tested using long term real-world data.
**Reproducibility:** our code and data are available at [link upon acceptance]

*Keywords:* Structural Health Monitoring, Drive-by Health Monitoring, Finite Element Models, Neural Net, Highway Bridge, Transportation Infrastructure.
*2010 MSC:* 00-01, 99-00

## 1. Introduction

Maintaining transportation networks is essential to supporting national security, the economy, and public safety. Because of delayed maintenance and budget limitations, however, bridges that are critical to a transportation network are in a state of disrepair [1, 2]. Per the 2017 American Society of Civil Engineering report, approximately 240 thousand bridges in the United States have exceeded their 50-year service life, and over 56 thousand bridges have been classified as structurally deficient [1]. The situation in other countries is not much different [3]. Further delays in the maintenance of this vital infrastructure system poses a significant risk of bridge failures, which would threaten national security, cause further economic losses, and result in the loss of lives. As such, a more efficient and cost effective health monitoring and maintenance strategy would aid to improve the state of this failing system by optimizing the allocation of funds and resources to where they are most needed.

*Corresponding author
*Email addresses:* wrlocke@clemson.edu (William Locke), jsybran@clemson.edu (Justin Sybrandt), isafro@clemson.edu (Ilya Safro), sez@psu.edu (Sez Atamturktur)
[1]Glenn Department of Civil Engineering, Clemson University
[2]School of Computing, Clemson University
[3]Department of Architectural Engineering, Pennsylvania State University

Presently, time interval-based visual inspections are the accepted practice for monitoring bridge health. The National Bridge Inspection Policy regulates the procedures for these inspections and dictates that bridge inspections should be performed every two years [4]. Despite having been criticized for being both inefficient and ineffective, this policy has continued to be practiced nation wide. Firstly, it has been argued that using financial resources to inspect bridges less than ten years old is inefficient as young bridges often exhibit little degradation [5]. Additionally, lack of financial resources may cause owners to miss necessary inspections, with approximately 17000 bridges missing their deadline in 2006, of which approximately 2700 bridges were considered obsolete or deficient [6, 7]. Secondly, visual inspections are ineffective as they not only fail to detect certain types of damage, but also rely on subjective assessments that often lead to inconsistent, unrepeatable observations [5, 8, 9, 10]. Structural Health Monitoring (SHM) is an alternative approach that offers a solution to these issues.

SHM is the process of implementing a damage detection and characterization strategy for engineered systems. SHM has been adopted as an accepted practice in many engineering disciplines, and is gaining popularity for use in civil engineering [11]. The inclusion of an SHM system as part of an asset monitoring strategy allows for more informed life-cycle management decisions that can help extend the asset's service life [12, 13, 14]. In bridge health monitoring, an effective strategy typically uses multiple online sensors and intelligent diagnostics to continuously detect damage on a local and/or global scale [11, 15]. However, these types of SHM systems are not feasible for short to mid-span bridges because of associated costs [14, 16, 17, 18]. For example, the initial cost of installing a system on every short to mid-span bridge in the U.S. is estimated to be in the range of tens of billions of dollars [19]. The methodology is made more expensive by essential sensor maintenance that requires significant time and resources for site visits [17, 18]. To overcome these limitations, a mobile health monitoring strategy known as Drive-by Health Monitoring (DBHM) has been proposed [14].

DBHM, or indirect health monitoring as it has also been called, is the practice of using accelerometers attached to passing vehicles to detect damage induced changes in the dynamic response of bridges [14]. Because vehicles and bridges create a coupled system, vehicle acceleration data contains information about bridge frequencies that can be used as health indicators. This concept was first demonstrated by Yang et al. when they successfully detected bridge frequencies contained within vehicle acceleration data generated from numerical finite element (FE) simulations [17]. Lin and Yang later validated the concept experimentally when they successfully detected frequencies contained within the acceleration response of a cart as it was towed across the Da-Wu-Lun bridge in Taiwan [20]. The goal of this strategy is to be able to continuously monitor bridges in a more efficient, cost effective, and less labor-intensive manner than any other forms of SHM or inspection practice; however, before this goal can be obtained, variabilities introduced by operational and environmental factors need to be addressed to ensure the accuracy of the health assessment being reported.

Operational and environmental parameters, such as bridge deck surface roughness, vehicle speed, traffic, and temperature, have been known to mask or shift bridge frequencies in such a way that accurately classifying damage becomes very difficult [20, 21, 22]. Progressively rougher surface profiles introduce high amplitude noise that obscures the process of extracting bridge frequencies from a vehicle's dynamic response. Correspondingly, at higher vehicle speeds, surface roughness introduces high frequency vibrations that further complicate bridge frequency detection [20, 22]. Higher vehicle speeds also cause the spectral resolution of sensors to decrease and the extracted frequencies to shift away from their actual values [17, 20]. On-going traffic has been demonstrated to actually aid in the drive-by health monitoring paradigm by increasing the acceleration amplitude associated with extracted bridge frequencies [20, 22], but others note that traffic can also cause these frequencies to fluctuate by several percent as a result of vehicle masses altering the effective bridge mass [23, 24, 25]. Temperature has a similar effect, causing frequencies to fluctuate by several percent over a 24-hour period, and by an even larger magnitude throughout the year [21, 26, 27]. Researchers have been able to address these issues by using an assortment of signal processing, statistical, and machine learning techniques [14]. These solutions, however, do not consider the cumulative effects of the aforementioned parameters and, therefore, cannot account for all the variation observed in real-world frequency data, which can potentially cause misidentifying damage. In this paper, we propose a method for assessing bridge health, while considering the cumulative effects of various operational and environmental factors.

To evaluate the feasibility of using raw vehicle frequency data to reliably detect the health of bridges when exposed to noise, numerical models that consider the cumulative effects of environmental and operational variabilities first need to be developed. Raw frequency data, along with other vehicle properties and temperature data, then need to be processed and analyzed using advanced machine learning algorithms to ascertain if an actionable health assessment can be reliably achieved.

In this study, we utilize a finite element methodology that represents the interaction between vehicles and bridges as a contact force to simulate simply supported, single-span bridges coupled with moving quarter-vehicle models [28]. A variety of different vehicles are simulated to represent daily traffic flow, while multiple bridges are simulated to represent variations that may exist across similar yet different structures. The number of different vehicles in this study represent a hypothetical scenario in which almost all vehicles crossing a bridge are outfitted with sensors to allow for the continuous monitoring of bridge health. Realistic representations of environmental and operational variabilities, along with bridge damage, are simulated by the models. To represent long-term natural variations in bridge frequency, we evaluate our models across two years of operational and environmental observations. Then, we leverage a multilayer neural network (NN) to capture a noise-tolerant relationship between sensor observations and bridge health. Input to the NN model is projected across a number of *layers*, each capturing an increasingly abstract representation of our input (e.g. frequencies, vehicle speed, temperature, etc.) when trained using stochastic gradient decent [29]. These layers are then projected down into a small set of "damage classes," each representing a different level of bridge health.

To explore the feasibility of NN models to predict bridge damage in the context of DBHM, we simulated twelve different data-collection scenarios and trained an NN on the data from each. These scenarios, while sharing the same basic bridge properties, varied in terms of environmental effects (present or absent), damage type (discrete or continuous), and the potential number of vehicles present on the bridge (one or two). For the case of simultaneous vehicles, we also varied whether we collected data from one or both vehicles. For each simulation scenario, we measured approximately 1,400 crossing each simulated day, across two simulated years. From the vertical acceleration data of each vehicle, we perform a Fast Fourier Transform to identify peak frequencies. Because we do not assume to know the exact values for each bridge's principle frequencies, but can estimate the range the frequencies may fall, we collect and observe the peaks within a predefined range; in this case the subject range encompassed the first ten peak frequency values. We additionally collect an estimate for a vehicle's mass and speed, as well as a measurement of the temperature. This forms a vector of 23 features — ten peak frequencies and corresponding acceleration amplitudes, mass, speed, and temperature — for every vehicle. We associate each of these measurements with the corresponding bridge health, which we discretized to six "damage classes."

In order to learn the mapping between observable features and bridge damage classes, we train a NN model per each of the twelve aforementioned scenarios using tensorflow [30]; the NN model learns to predict bridge health per-vehicle across both bridges. Then, each simulated day, we pool model predictions for a single bridge through majority voting in order to determine that bridge's estimated damage class. We evaluate our overall performance by studying the proportion of vehicles that agree with the ground-truth damage class against the incorrect damage class that received the most votes. Our evaluation shows that trends in these observable features can be generalized across multiple bridges.

This paper is organized as follows: Section 2 discusses the applied finite element method and includes parameter values for the bridge and vehicle models. Section 3 addresses simulating operational, environmental, and damage effects on the subject bridges; Section 4 discusses the NN and how it was applied towards the subject data; Section 5 discusses the outputs from the neural net and summarizes the results; and Section 6 summarizes our findings and provides suggestions for future research.

## 2. Finite Element Method for Vehicle-Bridge Interaction

### *2.1. FEM*

In this study, vehicle-bridge interactions are modeled using a finite element simulation based on the concept of vehicle-bridge interaction elements [28]; see Figure 1 for an example vehicle-bridge system. Because the majority of bridges in the United States are short-spanned (i.e. less than $50m$ $(160ft)$), and

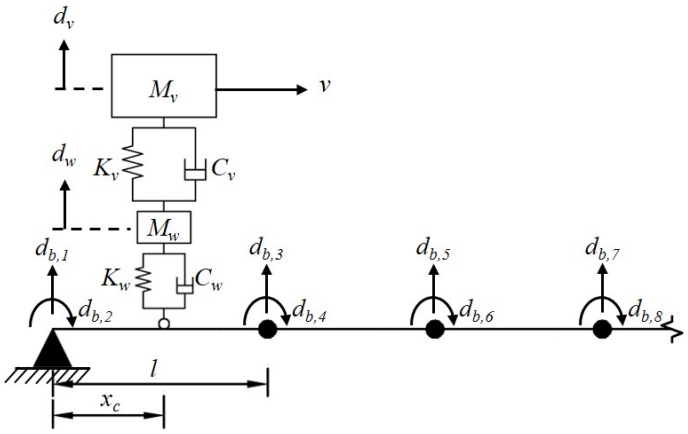


Figure 1: Quarter-vehicle model coupled with simply-supported bridge.

because most steel and concrete bridge designs can be employed using simply supported beams, each bridge is modeled as a short-spanned simply supported beam that is discretized into ten Euler-Bernoulli beam elements [31, 32, 33]. Equation 1 represents the equation of motion for an occupied beam element in the future time step $(t + \triangle t)$:

$$([m_{bi}]\{\ddot{d_{bi}}\} + [c_{bi}]\{\dot{d_{bi}}\} + [k_{bi}]\{d_{bi}\})_{t+\triangle t} = (\{f_{bi}\} - \{f_{bci}\})_{t+\triangle t}, \tag{1}$$

where $[m_{bi}]$, $[c_{bi}]$, and $[k_{bi}]$ represent the $i^{th}$ local element's mass, damping, and stiffness matrices, respectively. The column vectors $\{\ddot{d_{bi}}\}$, $\{\dot{d_{bi}}\}$, and $\{d_{bi}\}$ respectively indicate nodal acceleration, velocity, and displacement for the local element. The column vector $\{f_{bi}\}$ contains nodal external forces, while $\{f_{bci}\}$ is a column vector containing the nodal forces resulting from contact forces introduced by traversing vehicles.

Elemental matrices are pieced together to create the global structural matrices and external load vectors free of any vehicles. For this study, we implement a four degree-of-freedom stiffness matrix and a four degree-of-freedom continuous mass matrix. Because we are only interested in the modal frequency associated with vertical degrees-of-freedom, and because vehicles are assumed to travel at constant velocities, (i.e. do not introduce axial loads from acceleration) axial degrees-of-freedom are ignored. Additionally, Rayleigh damping is calculated using Eq. 2 below to determine the global damping matrix [34]:

$$[C_b] = b_0[M_b] + b_1[K_b] \tag{2}$$

$$b_0 = \xi\frac{2\omega_1\omega_2}{\omega_1 + \omega_2} \qquad b_1 = \xi\frac{2}{\omega_1 + \omega_2}, \tag{3}$$

where $[M_b]$, $[C_b]$, and $[K_b]$ represent a bridge's global mass, damping, and stiffness matrices, respectively. The parameters $b_0$ and $b_1$ are numerical constants calculated using the damping ratio $\xi$ and the first two undamped modal frequencies $w_1$ and $w_2$. The model frequencies are calculated using the eigen value function $eig([K_b], [M_b])$ in Matlab.

Once the global bridge matrices have been formulated, the next step is to calculate the global contact forces; this is done by first analyzing the equation of motion of the subject vehicle(s). Each vehicle is modeled as a two-degree-of freedom mass spring damper (i.e. quarter-vehicle), as seen in Figure 1. Equation 4 represents the equation of motion for a vehicle in the future time step $(t + \triangle t)$:

$$\left(\begin{bmatrix} M_v & 0 \\ 0 & M_w \end{bmatrix}\begin{Bmatrix} \ddot{d_v} \\ \ddot{d_w} \end{Bmatrix} + \begin{bmatrix} C_v & -C_v \\ -C_v & C_w + C_v \end{bmatrix}\begin{Bmatrix} \dot{d_v} \\ \dot{d_w} \end{Bmatrix} + \begin{bmatrix} K_v & -K_v \\ -K_v & K_w + K_v \end{bmatrix}\begin{Bmatrix} d_v \\ d_w \end{Bmatrix}\right)_{t+\triangle t} = \left(\begin{Bmatrix} f_{ve} \\ f_{we} \end{Bmatrix} + \begin{Bmatrix} 0 \\ f_{wc} \end{Bmatrix}\right)_{t+\triangle t}, \tag{4}$$

where $M_v$ and $M_w$ are the upper vehicle mass and wheel mass, respectively. $K_v$ and $C_v$ denote the stiffness and damping of the upper suspension system, while $K_w$ and $C_w$ denote the stiffness and damping properties of the wheel. Vectors $\{\ddot{d}\}$, $\{\dot{d}\}$, and $\{d\}$ receptively represent the vehicle's acceleration, velocity, and displacement. Vector $\{f_e\}$ contains external forces that act on both the vehicle body and wheel, while $f_{wc}$ indicates the vertical contact force acting on the wheel. To calculate the contact force, we first leverage Newmark Beta numerical integration to solve for the future acceleration, velocity, and displacement of the upper vehicle body; these values are calculated using Eq. 5-7:

$$\ddot{d}_{v,t+\triangle t} = a_0 \triangle d_v - a_1 \dot{d}_{v,t} - a_2 \ddot{d}_{v,t} \tag{5}$$

$$\dot{d}_{v,t+\triangle t} = \dot{d}_{v,t} + a_3 \ddot{d}_{v,t} + a_4 \ddot{d}_{v,t+\triangle t} \tag{6}$$

$$d_{v,t+\triangle t} = d_{v,t} + \triangle d_v, \tag{7}$$

where subscript $t$ indicates values for acceleration, velocity, and displacement in the present time step. The change in the upper vehicle displacement between the present and future time step is denoted by $\triangle d_v$. Constants $a_0 - a_4$ are used to perform the numerical integration; these values, along with others used later, are calculated in Eq. 8:

$$\begin{aligned} a_0 &= \frac{1}{\beta \triangle t^2} \quad a_1 = \frac{1}{\beta \triangle t} \quad a_2 = \frac{1}{2\beta} - 1 \quad a_3 = (1-\gamma)\triangle t \\ a_4 &= \gamma \triangle t \quad a_5 = \frac{\gamma}{t\beta} \quad a_6 = \frac{\gamma}{\beta} - 1 \quad a_7 = \frac{\triangle t}{2}\left(\frac{\gamma}{\beta} - 2\right), \end{aligned} \tag{8}$$

where $\beta$ $(\frac{1}{4})$ represent the variation in acceleration during the incremental time step $\triangle t$, and $\gamma$ $(\frac{1}{2})$ represents numerical or artificial damping introduced by discretization in the time domain [35]. In this study, the average acceleration method for Newmark Beta is utilized with a time step of a thousandth of a second (i.e. $\triangle t = .001$). Once the equations for the future vales are determined, they are entered into Eq. 4 to solve for the unknown change in upper vehicle body displacement $\triangle d_v$. The calculated change in displacement is then entered into Eq. 5-7 to solve for the future values.

After solving the equation of motion for the upper vehicle body in the future time step, we are able to solve the equation of motion for the wheel, and therefore calculate the contact force of the wheel. Using Newmark Beta method, the resulting equation for the wheel contact force is obtained:

$$f_{wc,t+\triangle t} = (M_c \ddot{d_w} + C_c \dot{d_w} + K_c d_w + P_c)_{t+\triangle t} + Q_{c,t}, \tag{9}$$

where $M_c$, $C_c$, and $K_c$ are respectively the contact mass, damping, and stiffness; while $P_{c,t+\triangle t}$ represents the effects of external forces on the vehicle, and $Q_{c,t}$ represents the effects of the vehicle's displacement vector at the beginning of the time step. Equations 10-14 indicate how these parameters are calculated:

$$M_c = M_w \tag{10}$$

$$C_c = (C_w + C_v) + \Psi_w \Psi_v^{-1} C_v \tag{11}$$

$$K_c = (K_w + K_v) + \Psi_w \Psi_v^{-1} K_v \tag{12}$$

$$P_{c,t+\triangle t} = -\Psi_w \Psi_v^{-1} f_{ve,t+\triangle t} - f_{we,t+\triangle t} \tag{13}$$

$$Q_{c,t} = \Psi_w \Psi_v^{-1} q_{v,t} - q_{w,t}, \tag{14}$$

where $\Psi_v$, $\Psi_w$, $q_{v,t}$, and $q_{w,t}$ are representative parameters used to simplify Eqs. 10-14, and are derived during the Newmark Beta integration; for more information on how these values are derived, please reference [28]. Equations 15- 18 indicate how these parameters are calculated:

$$\Psi_v = a_0 M_v + a_5 C_v + K_v \tag{15}$$

$$\Psi_w = -C_v a_5 - K_v \tag{16}$$

$$q_{v,t} = M_v(a_1 \dot{d_{v,t}} + a_2 \ddot{d_{v,t}}) + C_v(a_6 \dot{d_{v,t}} + a_7 \ddot{d_{v,t}}) - K_v d_{v,t} \tag{17}$$

$$q_{w,t} = -C_v(a_6 \dot{d_{v,t}} + a_7 \ddot{d_{v,t}}) + K_v d_{v,t}. \tag{18}$$

Using Eq. 19-21 below, the contact force in Eq. 9 is reformulated to be in terms of the occupied bridge element's nodal displacement, velocity, and acceleration:

$$d_w = \{N\}^T \{d_{bi}\}_{t+\triangle t} \tag{19}$$

$$\dot{d_w} = \{\dot{N}\}^T \{d_{bi}\}_{t+\triangle t} + \{N\}^T \{\dot{d_{bi}}\}_{t+\triangle t} \tag{20}$$

$$\ddot{d_w} = \{\ddot{N}\}^T \{d_{bi}\}_{t+\triangle t} + \{\dot{N}\}^T \{\dot{d_{bi}}\}_{t+\triangle t} + \{N\}^T \{\ddot{d_{bi}}\}_{t+\triangle t}, \tag{21}$$

where $\{N\}$ is a column vector containing Cubic Hermitian polynomial shape functions (i.e. the same functions used to derive the elemental stiffness matrix) [36]. Equation 22 indicates the vector of shape functions:

$$\{N\} = \left\{1 - 3x_b^2 + 2x_b^3; \quad x_c(1 - 2x_b + x_b^2); \quad 3x_b^2 - 2x_b^3; \quad x_c(x_b^2 - x_b)\right\}, \tag{22}$$

where $x_c$ is a vehicle's local position on an element, and $x_b$ is the local coordinate on an element (i.e. $x_b = \frac{x_c}{l}$). To transform the contact force to be in terms of the equivalent nodal forces ($\{f_{bci}\}$), the previously reformulated contact force is multiplied by the transpose of the aforementioned shape functions. Equation 23 shows the final equation of motion for an occupied bridge element (VBI element) with the derived $\{f_{bci}\}$ included:

$$\begin{aligned}([m_{bi}]\{\ddot{d_{bi}}\} + [c_{bi}]\{\dot{d_{bi}}\} + [k_{bi}]\{d_{bi}\})_{t+\triangle t} = \\ (\{f_{bi}\} - [M_c^*]\{\ddot{d_{bi}}\} - [C_c^*]\{\dot{d_{bi}}\} - [K_c^*]\{d_{bi}\} - \{P_c^*\})_{t+\triangle t} - \{Q_c^*\}_t,\end{aligned} \tag{23}$$

where the asterisked matrices and vectors are the parameters calculated in Eq. 10-14 that have been multiplied by the shape functions in Eq. 22.

Having obtained the finalized equation of motion for the VBI element, we add the modified contact matrices into the elemental matrices on the left and then assemble the local element matrices and vectors into the previously assembled global matrices at their respective global coordinates. Newmark Beta method is then utilized to solve for the global acceleration, velocity, and displacement vectors for the future time step $(t + \triangle t)$. The nodal acceleration, velocity, and displacement values for occupied elements are then substituted into Eq. 19-21 to calculate the future values for the wheel(s); the resulting values are then substituted into the vehicle's equation of motion Eq. 4 to calculate the future acceleration, velocity, and displacement values for the upper vehicle body. Once the future accelerations, velocities, and displacements are known for the vehicle(s) occupying the bridge, the global and local positions for the vehicle(s) are updated for the next time step and the analysis is performed again. This iterative process is repeated until the vehicle(s) reach the end of the bridge.

### *2.2. Bridge and Vehicle Properties*

In this study, two similar simply supported bridges are subjected to dynamic loading by a selection of moving quarter-vehicle models; Table 1 indicates the structural properties for each bridge. The bridges are determined to be geographically located in Clemson, SC so that previously collected temperature data from the area can be utilized to model temperature effects. The monitoring period for each bridge is 724 days, approximately two years. During this time, one or two vehicles (one traveling each direction) make a crossing every minute of each day; this was done to ensure adequate data is available for the NN process in section 4.

An inventory of ten separate vehicles is utilized for monitoring the health of the subject bridges; Table 2 indicates the properties for each vehicle. Variable traffic patterns are simulated by randomizing the sequence used to determine which one or two vehicles are currently traversing the bridge. The order and time history for each vehicle entering/exiting the bridge is randomized for the two vehicle case to prevent false relationships from being learned by the NN. To introduce variations in bridge frequency and spectral resolution, vehicle speeds are randomized between $10\frac{m}{s}$ and $25\frac{m}{s}$ $(22.4mph - 56mph)$. Lastly, to account for changes in passengers and cargo, vehicle masses are allowed to vary by different degrees. For small vehicles ($< 1000kg$), the mass is allowed to vary by $\pm 50kg$; for medium sized vehicles ($< 9000kg$), the mass is allowed to vary by $\pm 500kg$; and for large vehicles ($\geq 9000kg$), the mass is allowed to vary by $\pm 1000kg$.

Table 1: Bridge structural properties

| | Length $m$ | Mass $\frac{kg}{m}$ | Elastic Modulus $\frac{GN}{m^2}$ | Moment of Inertia $m^4$ | Damping Ratio % |
|---|---|---|---|---|---|
| Bridge 1 | 15 | 28125 | 35.00 | 0.5275 | 2 |
| Bridge 2 | 17 | 27155 | 35.75 | 0.8226 | 2.5 |

Table 2: Vehicle dynamic properties

| | Vehicle Mass $kg$ | Wheel Mass $kg$ | Suspension Stiffness $\frac{kN}{m}$ | Wheel Stiffness $\frac{kN}{m}$ | Suspension Damping $\frac{N \cdot s}{m}$ | Wheel Damping $\frac{N \cdot s}{m}$ |
|---|---|---|---|---|---|---|
| V1 | 375 | 60 | 15 | 200 | 1425 | 7 |
| V2 | 400 | 40 | 21 | 150 | 1500 | 50 |
| V3 | 800 | 87.15 | 66.82 | 101.12 | 1190 | 14.6 |
| V4 | 1200 | 140.4 | 18.62 | 101.12 | 1000 | 14.6 |
| V5 | 4000 | 550 | 320 | 1700 | 10000 | 610 |
| V6 | 4500 | 650 | 570 | 3000 | 21000 | 885 |
| V7 | 8000 | 1000 | 400 | 1750 | 10000 | 700 |
| V8 | 9300 | 700 | 400 | 1750 | 10000 | 650 |
| V9 | 10000 | 1000 | 100 | 3500 | 20000 | 900 |
| V10 | 11000 | 1000 | 280 | 8800 | 50000 | 1500 |

## 3. Modeling Operational, Environmental, and Damage Effects

### *3.1. Surface Roughness Profile*

Surface roughness can alter the acceleration response of a vehicle in a manner that may mask all bridge frequencies. In this paper, we generate a bridge's surface roughness profile using power spectral density (PSD) functions defined by ISO-8608:1995 standards. To use these standards, it is assumed the entire surface of a bridge deck falls under the same statistical classification, meaning a single roughness class exists homogeneously across the entire deck [37]. There are eight classes used to describe surface roughness; the first class (A) represents a smooth profile with minimal roughness, while the last class (H) represents a poor profile with high roughness [38]. In this project, the class A surface profile is applied towards each bridge to ensure that the selected NN strategy is at least feasible for the most optimal surface conditions.

Surface profiles are classified based on their PSD of vertical displacement ($G_D$), which is a function of spatial frequency ($n\frac{cycles}{m}$). Equation 24 defines $G_D(n)$ for a simulated surface profile:

$$G_D(n_j) = G_D(n_0)(n_i/n_0)^{-2}, \tag{24}$$

where $n_j$ represents the $j^{th}$ spatial frequency being considered within a predefined frequency range ($1\frac{cycle}{m}$ to $\frac{N}{L}\frac{cycles}{m}$); $N$ is the total number of data points and $L$ is the length of the bridge. $G_D(n_0)$ represents the PSD of vertical displacement calculated as a function of traditional values of spatial frequency ($n_0 = .1\frac{cycles}{m}$) [38, 39]. The ISO-8608 standard differentiates between surface classes based on their lower and upper bounds for $G_D(n_0)$; for surface class A, the lower and upper bounds are $0m^3$ and $32 \cdot 10^{-6}m^3$, respectively. In this study, the value for $G_D(n_0)$ is randomly selected between these bounds for each bridge simulation. The surface amplitudes are calculated in Eq. 25, and then entered into Eq. 26 to determine elevations at measurement points along the bridge:

$$A_j = \sqrt[2]{2G_D(n_j)\triangle n} \tag{25}$$

$$h(x) = \sum_{j=0}^{N}(A_i\cos(n_j x + \phi_j)), \tag{26}$$

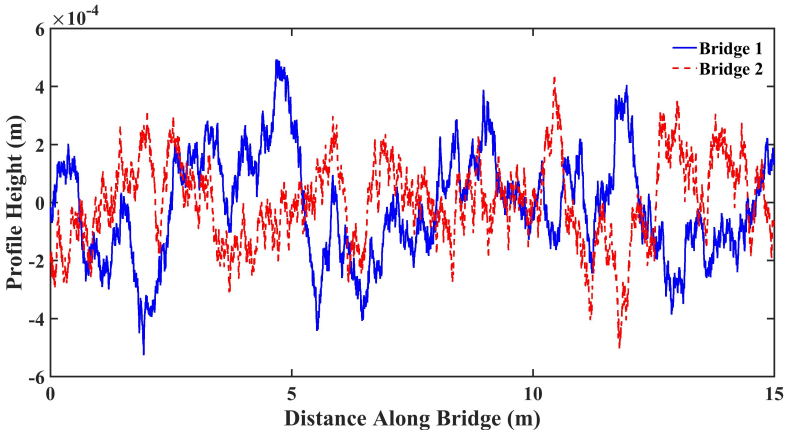


Figure 2: Surface elevations along bridge deck.

where $\phi_j$ is a random phase angle following a uniform probabilistic distribution between the values 0 and $2\pi$. Parameter $x$ is the global position within the range 0 to $L$, and $\triangle n$ represents the sampling interval of the spatial frequency calculated by taking the difference between the upper ($\frac{N}{L}\frac{cycles}{m}$) and lower ($1\frac{cycles}{m}$) spatial frequency values and dividing by $N-1$ [38, 39].

Vehicle velocity and modeling time-step govern the number of elevation points in a surface profile. For a fixed time-step, an increase in velocity decreases the number of elevation points, and a decrease in velocity increases the number of elevation points. In this paper, velocity is varied between $10\frac{m}{s}$ and $25\frac{m}{s}$ ($22.4mph - 56mph$), making it difficult to simulate a homogeneous profile that has consistent global elevations across test runs. What's more, the randomly assigned phase angle $\phi_j$ and the randomly sampled $G_D(n_0)$ further increase elevation variabilities across simulations, Figure 2 demonstrates this issue as the surface profiles for each bridge simulation are different despite being generated with the same vehicle speed. To prevent surface profiles from continuously changing across simulations, a single surface profile is generated for each bridge that can be applied towards all test runs regardless of vehicle speed. This is done by employing a velocity of $1\frac{m}{s}$ and a modeling time-step of $.001s$ to obtain surface elevations for every thousandth of a meter along the subject bridge's surface. By having such a fine surface mesh, the precise elevation corresponding to any vehicle's global coordinate on a bridge can be extracted for each time-step. If a surface profile was plotted for each vehicle crossing, it would be observed that the number of recorded elevation points still varies with vehicle speed, but now the elevation magnitudes would be the same for measurements occurring at the same global position. As mentioned, the elevation magnitudes are similar for each bridge profile, but the profiles are not the exact same due to the random phase angle and $G_D(n_0)$ values. This is to add a degree of variability that would exist when training an NN on two different yet similar bridges.

Surface roughness effects are integrated into the finite element model by altering the equations for wheel displacement, velocity, and acceleration (Eq. 19-21), and by altering the finalized equation of motion for the VBI element (Eq. 23). Equations 27-30 show these new calculations:

$$d_w = \{N\}^T\{d_{bi}\}_{t+\triangle t} + h(x) \tag{27}$$

$$\dot{d_w} = \{\dot{N}\}^T\{d_{bi}\}_{t+\triangle t} + \{N\}^T\{\dot{d_{bi}}\}_{t+\triangle t} + vh'(x) \tag{28}$$

$$\ddot{d_w} = \{\ddot{N}\}^T\{d_{bi}\}_{t+\triangle t} + \{\dot{N}\}^T\{\dot{d_{bi}}\}_{t+\triangle t} + \{N\}^T\{\ddot{d_{bi}}\}_{t+\triangle t} + v^2h'(x) \tag{29}$$

$$\Big([m_{bi}]\{\ddot{d_{bi}}\} + [c_{bi}]\{\dot{d_{bi}}\} + [k_{bi}]\{d_{bi}\}\Big)_{t+\triangle t} = \Big(\{f_{bi}\} - [M_c^*]\{\ddot{d_{bi}}\} - [C_c^*]\{\dot{d_{bi}}\} - [K_c^*]\{d_{bi}\} - \{P_c^*\} + \{H_c^*\}\Big)_{t+\triangle t} - \{Q_c^*\}_t \tag{30}$$

Table 3: Mean and standard deviation for temperature variables

| | $Q$ | $S$ | $R$ | $\gamma$ | $\tau$ |
|---|---|---|---|---|---|
| Mean | 1.0129 | −0.0048 | 0.1977 | −1.1012 | 3.1466 |
| STDV | 0.003 | 0.0001 | 0.0027 | 0.0513 | 0.0861 |

where $v$ is the velocity of the vehicle, and $h'(x)$ is the derivative of the surface amplitude with respect to $x$. Vector $\{H_c^*\}$ represents the effect of surface roughness in the contact force between the vehicle and bridge, and is calculated using Eq. 31 below:

$$\{H_c^*\}_{t+\triangle t} = \{N\}\left(v^2 M_c h''(x) + v C_c h'(x) + K_c h(x)\right). \tag{31}$$

*3.2. Temperature Effects*

In this section, focus is placed on modeling temperature induced variations in DBHM data. Thermodynamics indicate that a linear correlation exists between temperature and bridge elastic modulus/ natural frequency [40], a trend that researchers have found holds true for many reinforced concrete decks [41, 42]. However, bi-linear relationships have also been observed for bridges where an asphalt wearing surface causes different rates of softening and stiffening, such as the case of the Z-24 bridge in Switzerland, or where interior moisture freezing causes deck stiffness to increase at a linear rate different than softening, such as the case of the Dowling Hall Footbridge at Tuffs University [26, 27]. Thus the relationship between temperature and bridge modulus/ frequency can be linear or nonlinear in nature, and is dependent upon a bridge's environmental and operational conditions.

Because the constitutive equations required to simulate the governing relationship between temperature and a bridge's dynamic characteristics are mostly unknown, and the number of parameters that must be considered is vast, simulating thermodynamic effects is a difficult task [43, 44]. To get around this, models based on measurements from real structures can be leveraged to portray the relationship between temperature and variations in a bridge's dynamic response [44]. In this paper, we apply bi-linear equations for bridge elastic modulus developed for the Dowling Hall Footbridge [45]. Equation 32 calculates the modification factor for a subject bridge's elastic modulus, which is then multiplied to the bridge modulus to obtain the temperature shifted modulus value [45]:

$$\Theta = Q + ST_t + R\left(1 - \text{erf}\left(\frac{T_t - \kappa}{\tau}\right)\right) \tag{32}$$

$$E_m = \Theta E_0, \tag{33}$$

where $Q$ and $ST_t$ are hyperparameters that represent the linear behavior of the bridge above freezing, while $R(1 - \text{erf}(\frac{T_t-\kappa}{\tau}))$ represents the linear behavior below freezing; erf indicates the error function in Matlab. $T_t$ is the temperature at time $t$, while variables $\kappa$ and $\tau$ are hyperparameters that represent the area for transitioning from below freezing to above freezing. $E_0$ is the nominal bridge elastic modulus. Table 3 shows the mean and standard deviation values for each variable [45]. Although these equations were developed for a specific bridge, they are deemed appropriate for our study as the deck of the Dowling Hall Footbridge is constructed using a traditional reinforced concrete design with no wearing surface, analogous to most highway bridges in the United States.

In this study, we leverage hourly temperature data provided by the National Centers for Environmental Information for the city of Clemson, SC to create realistic daily and yearly oscillation patterns in bridge elastic modulus/ frequency [46]. Linear interpolation provides temperature values for simulations occurring between the top and bottom of each hour. Because each bridge is short-spanned, it is assumed they have consistent exposure conditions, and therefore uniform temperatures throughout. It is also assumed that temperature does not affect the dynamic properties of the vehicles, and that damage does not cause a change in the bi-linear relationship between temperature and bridge modulus.

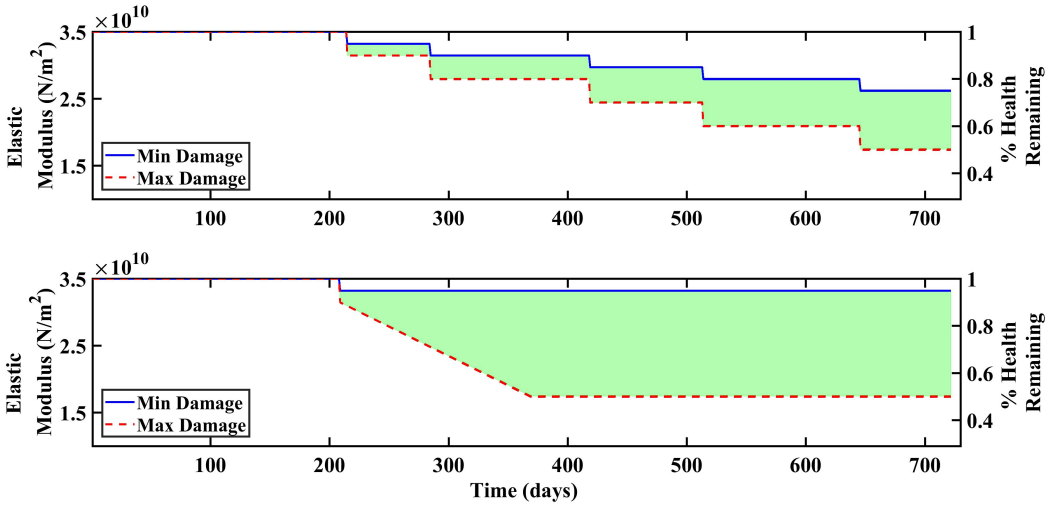


Figure 3: Damage envelopes for the discrete damage case (top) and the continuous damage case (bottom). Note that both the time and severity of each damage event is randomly determined for each simulation experiment.

### *3.3. Modeling Damage*

We introduce two different damage cases in this project, a discrete damage case and a continuous damage case. In the discrete damage case, damage is introduced as five levels of instantaneous decreases in stiffness (i.e. elastic modulus) for the same randomly selected location on the subject bridge. Each level of damage corresponds to a reduction, between five to ten percent of the nominal stiffness capacity, in the present capacity. The upper and lower bounds in Figure 3 indicate the maximum (50 percent) and minimum (25 percent) levels of elastic modulus reduction for the discrete damage case, while the shaded region is an envelop representing all the possible levels of damage that can exist between these extremes. The initial decrease in elastic modulus randomly occurs between 182 to 243 days through the two year monitoring period. The remaining decreases in elastic modulus sporadically occur between 255 to 328 days, 401 to 474 days, 511 to 547 days, and 584 to 657 days through the two year monitoring period. These ranges of time were chosen to add a degree of uncertainty to the model, preventing the NN from learning fake relationships about when damage should occur next. Temperature effects are still considered for the damaged bridge element, with the modification factor now adjusting the damaged elastic modulus value.

In the continuous case, the initial damage is also introduced as an instantaneous decrease in stiffness for a randomly selected location on the subject bridge; however, after the initial stiffness reduction, the selected bridge element can continue to loose capacity daily. Like the discrete case, the initial reduction in stiffness is caused by a decrease in elastic modulus between five to ten percent of the original nominal capacity, and occurs randomly between 182 to 243 days through the two year monitoring period. After the initial damage, a random number generator is used to determine if the the bridge element experiences further degradation each subsequent day. The subject element has the potential to degrade daily by up to a quarter of a percent of the original nominal capacity. According to the bottom image of Figure 3, the minimum level of damage that can occur for this case is a five percent reduction in elastic modulus, while the maximum level of damage that can exist is a 50 percent reduction in elastic modulus. The shaded region represents an envelop of all the possible damage levels that can occur during the continuous damage case. Again, temperature effects are still considered for the damaged bridge element. Because location, time, and severity of damage are randomly determined for both cases, an extra degree of variability exist when applying the trained NN model to the similar-yet-different bridges. This creates a real-world scenario that could exist if two identical bridges were being monitored.

## 4. Machine Learning Implementation Details

### *4.1. Machine Learning Problem Formulation*

Despite being one of the most popular indicators for bridge damage, changes in natural frequencies caused by damage tend to be small and are often masked by operational and environmental noise [14]. These limitations suggest that NNs, which can provide fast inferences as well as noise-tolerant approximate results, could be an effective solution strategy. In many other application areas, neural networks have been shown to effectively approximate complex simulations [47, 48]. In these cases, a computationally expensive routine has been replaced by a reasonably high-quality approximation, which reduces the overall time-to-solution by multiple orders of magnitude. Similar networks are also noise-resilient across a number of tasks, such as computer vision [49]. Techniques such as dropout [50] and stability training [51], explicitly enhance the ability of these networks to generalize. The former simply "drops" a fraction (typically 50%) of the input features randomly per-example. Doing so deemphasizes spurious correlations across the modified input data, which in turn leads to a more resilient machine learning model. The latter perturbs input data through a number of predetermined filters, consisting of algorithmic modifications as well as various noise distributions. Again, this approach leads to more resilient model because small modifications to input should be less able to cause big changes in output. In the case of DBHM, we apply similar techniques to quantify bridge health given noisy readings from vehicle-mounted sensors.

### *4.2. Feature Engineering*

In machine learning, a "feature" refers to an observable characteristic of something we would like to model [52]. Ultimately, a machine learning model must learn the relationship between these observable characteristics and some resulting characteristic of interest. In our case, we must select the features that allow us to estimate bridge health. We are limited by the drive-by monitoring paradigm to only select features that could be observed via sensors placed in a moving vehicle. We assume a monitoring vehicle will have an accelerometer capable of capturing vertical acceleration, a thermometer to capture ambient temperature, and a speedometer to measure average speed. Additionally, because we cannot know the exact mass of each vehicle due to variable cargo and passengers, we approximate vehicle masses to be the values provided in Table 2. This is equivalent to the real-world scenario where vehicle mass could be approximated as the value provided by a vehicle's manufacturer.

We preprocess the sequence of vertical accelerations by first performing an FFT to identify peak frequencies. Because we assume no prior knowledge of a bridge's dynamic properties, we do not know the exact values of the modal frequencies we wish to observe. However, we are able to approximate a bridge's first principle frequency using the equation below [53]:

$$f_1 = 100/L. \tag{34}$$

Because Eq. 34 only provides a reasonable estimate of a bridge's principle frequency, and because environmental and operational noise introduce variations in the frequency response spectrum, we collect and observe $k$ peaks within a predefined band around the calculated principle frequency value. For this analysis, the predefined band corresponds with the first ten peak frequencies (i.e. $k = 10$). Here we define a "peak" to be any frequency that corresponds to a locally maximal amplitude. We note that other, more sophisticated, approaches may be able to identify important peaks [54], smooth noise in the FFT [14], or even learn from the raw vertical acceleration sequence directly [55]. We leave the use of more advanced signal-processing approaches for future work.

Additionally, there are a number of potential features we omit in order to ensure a model that can generalize to different vehicle and bridge configurations. These features can be grouped into two classes, those that are observable but not helpful, and those that are helpful but not observable. The former group consists of features such as the time of day or year a vehicle is present on a bridge. If time were included, the NN model would most likely learn a linear inverse correlation between time and health, and in doing so would discard all other information. Clearly, this would not be a preferable model. The latter group of features, those that we cannot observe, include bridge properties such as mass and surface elevations. While

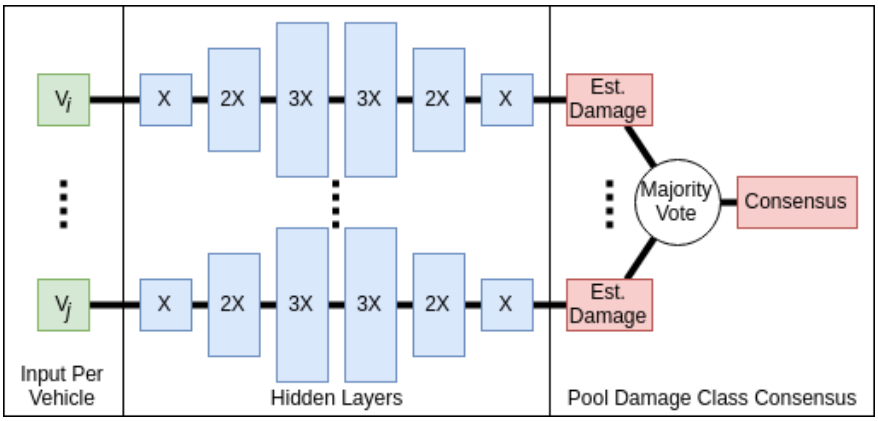


Figure 4: Above depicts the neural architecture at inference time. Each box represents a layer, and the lines represent the left-to-right flow of data. Each vehicle's ($X = 23$) features are input to the six layer architecture to gain a confidence score per damage class. We record the most-confident damage class for each vehicle, and then accept a consensus answer among the vehicles.

these features would certainly improve our model, we do not assume they are detectable from a vehicle outfitted with the aforementioned health monitoring sensors.

In Figure 4 we depict the neural architecture used to determine bridge health for each simulated "day." First, we collect sensor data for each vehicle, shown in green. These readings for each vehicle individually is then projected through a six layer neural network. These layers are atypical as the intermediate layers increase in dimensionality. We observe that by expanding from our set of input features to a latent representation that is three-times larger, this model is capable of discovering useful higher-order features from our input. Finally, we estimate a damage class per-vehicle following those six layers, shown in red. Each vehicle on a given "day" is then pooled together to reach a consensus. Here we take a simple "majority vote," meaning that the model outputs whichever damage class is predicted most often among sensing vehicles.

### *4.3. Class Balancing*

Machine learning models have a tendency to under fit when training data contains an imbalance of labels [56]. In our simulation scenarios, we often have more damaged than "healthy" days, which becomes a further problem when we split those damaged days across five different damage classes. Without a balancing strategy it becomes likely that our ML model will attempt to predict that every day is the same as the largest label group, after all in the unbalanced scenario, that strategy leads to the greatest initial jump in performance. To dissuade our classifier from that local minimum, we perform a class balancing preprocessing step within our training data.

We balance damage classes by under or over sampling each class in order to maintain certain ratios between healthy and damaged conditions, as well as between each damage class. First this involves enforcing a 30:70 split between healthy days and damaged days. We observe this ratio encourages the model to detect the first instance of damage without over fitting. Then, within the set of damaged days we oversample underrepresented damage classes so that no class has fewer examples than 20% of the original damaged examples. The effect of this sampling is that we under sample healthy days, over sample some of the short-lived intermediate damage classes, and leave the terminal damage class, which is often the longest-lasting, untouched.

### *4.4. Evaluation Strategy*

To evaluate the performance of our NN, we use our previously discussed FE model to collect data for two different bridges across two simulated years. We vary the damage conditions (discrete or continuous damage), number of simultaneous vehicles (one or two), and the simulated environmental factors (enabled or disabled). Each simulated day consists of at least 1,400 vehicles of differing dynamic properties and speeds,

which allow us to define a daily "confidence" measure (different than the confidence of a single vehicle). Let $T_z$ be the true damage class of the considered bridge on day $z$. Let $P(d, z)$ be the proportion of vehicles on day $z$ that predict damage class $d$. Let $D$ be the set of damage classes. Then $C_z$, the confidence of our model on day $z$ is:

$$C_z = P(T_z, z) - \max_{d \in D - T_z} P(d, z). \tag{35}$$

Put plainly, $C_z$ is equal to one if every vehicle predicts the damage class accurately. $C_z$ is equal to zero if the number of vehicles predicting the correct damage class equal the number of vehicles predicting some incorrect class. $C_z$ is only less than zero if some other class is preferred to the true damage class. In our later analysis, we plot daily confidence over the course of our two simulated years to show the model's ability to detect bridge damage in different conditions.

## 5. Results

Using the same NN configuration described above, we evaluate our methodology across a number of simulation configurations. These modifiable parameters include: the number of simultaneous vehicles, the manner that damage is accumulated, and whether or not environmental factors affect a bridge's structural properties.

We vary the number of simultaneous vehicles present during a simulation run from one to two. In the case where two vehicles are present, we only collect sensor readings from a single vehicle. In addition, the unobserved vehicle may start before or after the observed vehicle, and it may also travel at any speed within the predefined range. As a result, the unobserved vehicle acts as a significant noise source that excites the bridge and disrupts the sensor readings of our observed vehicle.

We vary the manner that damage is accumulated in two ways, either damage occurs in multiple discrete steps or damage occurs continuously wherein every day the initial damage continues to worsen. As described above, each damage class corresponds to more granular ranges of structural health, such as each distinct damage event in the discrete case, or after a 10% change in overall health in the continuous case. In addition, we evaluate our NN model based on both its ability to detect *any* damage, as well as its ability to detect each specific "damage class." This corresponds to a two-class model in the former, and a multi-class model in the latter. We anticipate that a similar NN DBHM model in a real-world deployment scenario will likely be used in the two-class configuration, as decision makers are primarily concerned with the point at which some action must be taken. By extending our evaluation to the multi-class configuration, we evaluate our NN's ability to generalize, as well as its ability to detect the bridge-health signal from vibration peaks in a noisy environment.

### *5.1. Two-Class Damage Prediction*

In Table 4 we show the two-class results. For our metrics we define the presence of any damage as the "positive" class for the purpose of calculating precision, recall and F1 score. These metrics capture our NN's performance better than the typical accuracy metric in Eq. 36 because in the two-class scenario there are significantly fewer days the bridge spends healthy, which means the two-class evaluation is between unbalanced classes.

$$\text{Accuracy} = \frac{\#\text{ of days the model is correct}}{\#\text{ total days}} \tag{36}$$

$$\text{Precision} = \frac{\#\text{ of days the model } \textit{correctly} \text{ predicts the bridge is damaged}}{\#\text{ of days the model predicts the bridge is damaged}} \tag{37}$$

$$\text{Recall} = \frac{\#\text{ of days the model } \textit{correctly} \text{ predicts the bridge is damaged}}{\#\text{ of days bridge is actually damaged}} \tag{38}$$

Table 4: Results from our NN's *two-class* performance

| Num. Vehicles | Damage Type | Environmental Effects | Accuracy | Precision | Recall | F1 |
|---|---|---|---|---|---|---|
| 1 | Continuous | Disabled | 100.00% | 1.00 | 1.00 | 1.00 |
| 1 | Continuous | Enabled | 100.00% | 1.00 | 1.00 | 1.00 |
| 1 | Discrete | Disabled | 100.00% | 1.00 | 1.00 | 1.00 |
| 1 | Discrete | Enabled | 100.00% | 1.00 | 1.00 | 1.00 |
| 2 | Continuous | Disabled | 71.12% | 1.00 | 0.61 | 0.76 |
| 2 | Continuous | Enabled | 97.24% | 0.97 | 1.00 | 0.98 |
| 2 | Discrete | Disabled | 93.18% | 1.00 | 0.91 | 0.95 |
| 2 | Discrete | Enabled | 89.99% | 1.00 | 0.86 | 0.92 |

The above captures our NN's *two-class* performance, and ability to detect *any* amount of damage to a healthy bridge. Here, "Num. Vehicles" refers to the maximum number of simultaneous vehicles present during a crossing, "Damage Type" refers to the model used to determine ground-truth bridge damage, and "Environmental Effects" refers to whether or not the temperature effects described in Section 3.2 are used in the simulation. In the cases where these effects are disabled, all observations provided to the NN model contain a null value for temperature.

$$\text{F1} = \frac{2 \times \text{Precision} \times \text{Recall}}{\text{Precision} + \text{Recall}} \tag{39}$$

Based on the results in Table 4, we see that the model performs perfectly in any one-vehicle scenario. When looking at the four scenarios wherein a second vehicle acts as an additional noise source, we begin to see performance differences. See that the continuous damage scenario with environmental effects enabled is our strongest performer within the two-vehicle experiments, with the two discrete cases not far behind. A potential reason for the high performance of the continuous scenario is that the underlying model can observe far more damage scenarios over the course of the simulation — while the discrete case jumps between five different natural-frequency states, the continuous case iterates across hundreds. This, combined with environmental trends such as the yearly rise and fall of temperature, allow the model to distinguish bridge health from damage. In the reverse, the same continuous model performs poorly if environmental factors are disabled. This result is due to noise from the second vehicle overpowering the minute daily changes in bridge health. Without environmental effects to aid in untangling these effects, the continuous model under performs. Specifically, this leads to a decrease in accuracy of 26.12%, and a decrease in F1 of 0.22. In contrast, there are only minor differences in the discrete case, with a change in accuracy of only 3.19% and a change in F1 of 0.03.

### *5.2. Multi-class Damage Predictions*

To ensure that our model identifies reasonable trends in its provided peak frequencies, we compare performance across multiple bridge damage classes. In this evaluation we have six classes, one representing a healthy bridge, and five for each state of increasing damage. Because we no longer have a two-class problem, the previously defined metrics of precision, recall, and F1 score no longer apply directly. Instead, we look at overall accuracy where a day's prediction was accurate only if the predicted class agrees exactly with the true damage class. We compare performance in this respect across all previously established simulation scenarios, and now across two different simulated bridges. Table 5 summarizes the overall performance of these scenarios.

To evaluate the multi-class performance across specific scenarios, we generate confidence plots. For instance, the plot in Figure 5 describes the performance of our machine learning model in the one-vehicle, discrete damage, environmental effects enabled scenario on the first bridge. Along the top depicts the ground-truth damage class, ranging from D0 (healthy) to D5 (maximal damage). In the center is the prediction confidence per-day as defined in Equation 35. If the colored region is above zero, then the day's prediction aligns exactly with the ground truth. If the region is negative, the prediction was incorrect, and the color of that negative region corresponds to the incorrectly predicted class. We see in Figure 5 that we predict the correct damage class every day. Additionally we see high confidence across all days, representing that most vehicles correctly detect the exact classes of bridge damage.

Table 5: Results from our NN's *multi-class* performance

| Num. Vehicles | Damage Type | Environmental Effects | Bridge 1 Acc. | Bridge 2 Acc. |
|---|---|---|---|---|
| 1 | Continuous | Disabled | 98.26% | 98.26% |
| 1 | Continuous | Enabled | 98.40% | 98.40% |
| 1 | Discrete | Disabled | 87.08% | 85.20% |
| 1 | Discrete | Enabled | 95.36% | 94.34% |
| 2 | Continuous | Disabled | 61.54% | 59.07% |
| 2 | Continuous | Enabled | 87.08% | 93.76% |
| 2 | Discrete | Disabled | 85.34% | 78.52% |
| 2 | Discrete | Enabled | 82.44% | 86.79% |

The above demonstrates the performance of the NN on both bridges using the *multi-class* model. In these cases, high accuracy indicates that the NN model detects the exact damage class each day.

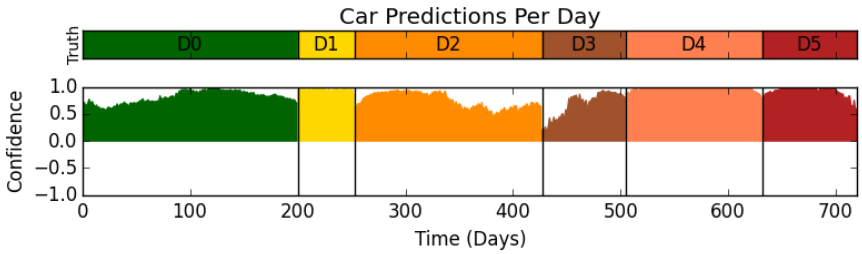


Figure 5: The above confidence plot describes the ability of approximately 1,400 vehicles to determine bridge health over the course of a two-year timespan. This model was trained using only data collected while the sensing car was alone on the bridge. In this damage scenario, five damage events occur sporadically, which act as discrete changes to bridge natural frequency. Environmental factors allow the ML model to counteract noise, leading to more accurate results.

In Figure 6 we depict the same simulation scenario *except* now an additional vehicle may be on the bridge. We see a distinct drop in overall confidence corresponding to this additional noise source, and we also see a number of days wherein the model inaccurately predicts damage class. For instance, we observe that the added noise blurs the line between D2 and D3 around day 425. Still, we see positive confidence for most days, with a clear distinction between damage and health. Again, any positive confidence value represents that the correct damage class is preferred to any other, so while confidence levels have decreased overall, the NN still detects the the correct health a large majority of days.

Figure 7 follows the same simulation configuration as Figure 5, *except* this plot uses the continuous damage model. As opposed to before, we now see a more gradual rise and fall of confidence in damage classes 1,2, and 3. Damage class 4 has a similar pattern, although the model detects class 5 earlier than it should. This represents the slow accumulation of damage, while over time, more and more vehicles predict the previous damage class and begin to identify the new one.

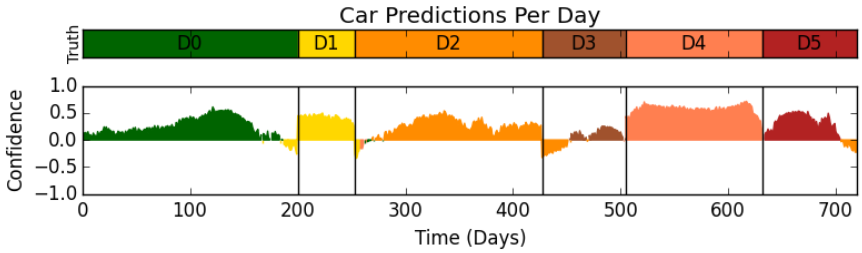


Figure 6: The above depicts the same damage and environmental scenario as Figure 5, except now a second car be present during data collection. Because we do not assume any communication apparatus or camera, our model does not directly account for the other vehicle. While confidence does decrease, we see that the overall trend is still able to identify damage consistently.

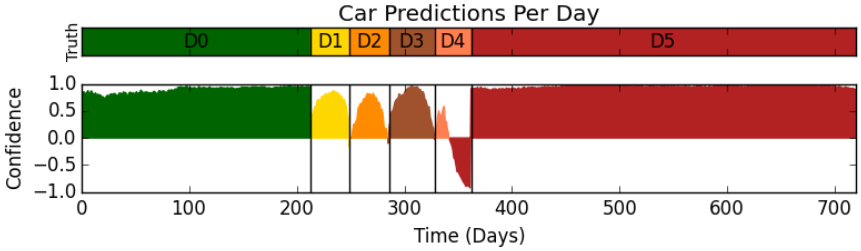


Figure 7: The above depicts the same damage and environmental scenario as Figure 5, except now we assume that damage is chronic and accumulates over time. For a fair comparison, our model still must place bridge health into either the healthy category, or one of the five damage categories. In this scenario we see that the bridge's health deteriorates faster, and the model is able to pinpoint these trends for a majority of classes over time.

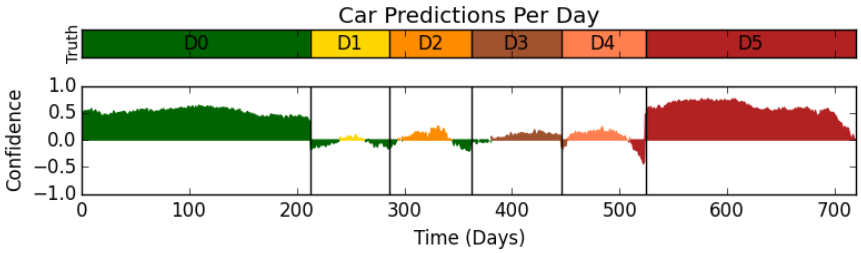


Figure 8: The above depicts the same scenario as Figure 7, except an additional vehicle may be present on the bridge during the sensor readings. We see that the combination of the second car along with the challenges of the continuous damage model are a challenge for this model in the intermediate damage classes. Yet, while the certainty may be low, the consensus is still correct on a majority of days.

Introducing the noise of an additional vehicle to the previously discussed scenario results in Figure 8. Clearly, this added noise source reduces the performance of our overall model, primarily seen in the low confidence for damage classes one through four. The boundaries are even harder to distinguish, as the continuous damage model's slow changes are blurred further by noise. Yet still the larger classes D0 and D5 are much easier to identify as their size leads to a larger incentive for the neural network.

## 6. Conclusion

The intent of this study was to investigate the viability of the DBHM paradigm when subjected to the combined effects of environmental and operational variabilities. In this study, we used a finite element methodology based on the concept of vehicle-bridge interactions to simulate two simply supported bridges subjected to dynamic loads introduced by moving quarter-vehicle models. Environmental and operational noise were represented in the models in the form of vehicle traffic, surface roughness, and temperature induced changes in bridge elastic modulus. Damage was introduced randomly as either an instantaneous or gradual decrease in the elastic modulus of a single bridge element. As damage is known to cause variations in bridge frequencies, we extracted the frequency content contained within the acceleration response of each vehicle. Because operational and environmental effects can introduce high amplitude noise or shifts in the frequency response spectrum, it is difficult to distinguish between what is a bridge's modal frequency or noise. To account for this, a range of peak frequency values had to be extracted from the frequency response data. We then utilized a multi-layer NN to analyze the subject frequency range and provide noise-tolerant approximations of each bridge's health condition. Two separate studies were conducted to evaluate the performance of our NN model. The first study was based on a two-class system in which each structure was classified as healthy or damaged, this represented the real-world scenario where decision makers are primarily concerned about whether or not actions need to be taken. The second study was based on a

multi-class system in which each structure was classified based on the level of theorized damage, this tested the NN's ability to generalize and provide insight into how well the method performed under noise.

From the two class study, we were able to discern that the monitoring strategy performed perfectly for both damage scenarios when vehicle traffic was absent during the monitoring process. Additionally, we saw a negligible decrease in performance for both damage scenarios when multiple vehicles were present on the bridge at the same time. This indicated that the methodology could serve as a viable option for evaluating whether or not a subject bridge needs to be inspected; however, no information can be provided as to the magnitude of damage. From the multi-class study, we determined that the magnitude of damage could be accurately identified for cases where only a single vehicle was present during data acquisition and damage was sporadic and instantaneous. For cases where a single vehicle was present and damage was gradual, we saw roughly the same level of classification accuracy with only a few miss-classifications. These miss-classifications were negligible, however, as they occurred at the boundaries between classes where noise may be more prevalent. This was found to be the same for damage scenarios where vehicle traffic was also present. The multi-class study indicated the viability of the methodology to provide decision makers with information about the severity of damage, allowing the decision to be made about whether or not an inspection and/or repair is required.

## 7. Future Work

The finite element simulations in this study are idealistic representations of actual bridge conditions, and therefore do not consider all of the sources of noise that could potentially exist in a real-world environment. The results from this study, however, indicate that the developed methodology can serve as a viable health monitoring strategy and should be further tested on real-world data. Future research will need to be conducted on data collected directly from physical bridges and vehicles to determine if damage detection is feasible in the real-world. For instance, we simulate over 1,400 daily bridge crossings, but this may not be realistic for all short to mid-spanned bridges. A further computational study ought to be conducted in parallel with physical testing to ascertain the minimum range of daily traffic required for accurate damage classification. Furthermore, a study will need to be conducted to evaluate the effectiveness of the methodology for rougher surface profiles.

Going forward, future research should also focus on extracting a variety of different features, other than frequency, to compare against each other and determine the most optimal damage indicator. To determine the most optimal damage indicator out of the selected subset of features, a variety of different damage types should be investigated (e.g. propagating breathing cracks, changes in boundary conditions, and degrading surface roughness). Research should also be conducted to determine if leveraging different signal processing, statistical models, and machine learning algorithms help to not only increase detection accuracy, but also distinguish between damage types.

To capture more intricate and time-dependent relationships within in our machine learning framework, we anticipate that more complex models such as the Long Short-Term Memory (LSTM) neural architecture [55] may improve performance. This recurrent model processes time-series information and would adapt its predictions based on what it had previously observed. We anticipate that this model would improve the few times that our present model incorrectly identifies that the bridge is healthier than it was previously. However, the primary contribution on this work is the proof-of-concept that vehicle-based signals can lead to accurate bridge-health predictions.

## Acknowledgements

The authors gratefully acknowledge the support of the National Science Foundation under grant #1633608.

## References

[1] ASCE, Report card of america's bridge infrastructure 2017.

[2] R. Young, Transportation infrastructure: An overview of highway systems and south carolina's position and status, Institute for Public Service and Policy Research, University of South Carolina.
[3] K. Willsher, L. Tondo, J. Henley, Bridges across Europe are in a dangerous state, warn experts, The Guardian.
[4] F. H. A. FHWA, National bridge inspection standards (nbis), Federal Register 69 (239) (2009) 74438.
[5] A.-H. G. ASCE/SEI-AASHTO, White paper on bridge inspection and rating, Journal of Bridge Engineering 14 (1) (2009) 1–5.
[6] B. Dedman, Late inspections of bridges put travelers at risk, MSNBC Jan 30.
[7] E. McNichol, It's time for states to invest in infrastructure, Washington DC: Center on Budget and Policy Priorities.
[8] K. Hover, Special problems in evaluating the safety of concrete bridges and concrete bridge components, Construction and Building Materials 10 (1) (1996) 39–43.
[9] M. Moore, B. Phares, B. Graybeal, D. Rolander, G. Washer, Reliability of visual inspection for highway bridges, Federal Highway Administration 1 (FHWA-RD-01-020).
[10] B. Phares, G. Washer, D. Rolander, B. Graybeal, M. Moore, Routine highway bridge inspection condition documentation accuracy and reliability, Journal of Bridge Engineering 9 (4) (2004) 403–413.
[11] C. Farrar, K. Worden, An introduction to structural health monitoring, Philosophical Transactions of the Royal Society of London A: Mathematical, Physical and Engineering Sciences 365 (1851) (2007) 303–315.
[12] M. Feng, Long-term structural performance monitoring of bridges: Phase ii: Development of baseline model and methodology for health monitoring and damage assessment.
[13] A. Gastineau, T. Johnson, A. Schultz, Bridge health monitoring and inspections–a survey of methods, Minnesota Department of Transportation.
[14] A. Malekjafarian, P. McGetrick, E. OBrien, A review of indirect bridge monitoring using passing vehicles, Shock and vibration 2015.
[15] F. Chang, A summary of the 3rd workshop on structural health monitoring, Tech. rep., Stanford University CA. Dept of Aeronautics and Astronautics (2002).
[16] A. Aktan, A. Helmicki, V. Hunt, Issues in health monitoring for intelligent infrastructure, Smart Materials and Structures 7 (5) (1998) 674.
[17] Y. Yang, C. Lin, J. Yau, Extracting bridge frequencies from the dynamic response of a passing vehicle, Journal of Sound and Vibration 272 (3-5) (2004) 471–493.
[18] J. Lynch, K. Loh, A summary review of wireless sensors and sensor networks for structural health monitoring, Shock and Vibration Digest 38 (2) (2006) 91–130.
[19] J. Lynch, Smart bridges: Expert q/a.
[20] C. Lin, Y. Yang, Use of a passing vehicle to scan the fundamental bridge frequencies: An experimental verification, Engineering Structures 27 (13) (2005) 1865–1878.
[21] C. Farrar, S. Doebling, P. Cornwell, E. Straser, Variability of modal parameters measured on the alamosa canyon bridge, Tech. rep., Los Alamos National Lab., NM (United States) (1996).
[22] Y. Yang, W. Chen, H. Yu, C. Chan, Experimental study of a hand-drawn cart for measuring the bridge frequencies, Engineering Structures 57 (2013) 222–231.
[23] C. Kim, D. Jung, N. Kim, S. Kwon, M. Feng, Effect of vehicle weight on natural frequencies of bridges measured from traffic-induced vibration, Earthquake Engineering and Engineering Vibration 2 (1) (2003) 109–115.
[24] J. Li, M. Su, L. Fan, Natural frequency of railway girder bridges under vehicle loads, Journal of Bridge Engineering 8 (4) (2003) 199–203.
[25] S. Khan, S. Atamturktur, M. Chowdhury, M. Rahman, Integration of structural health monitoring and intelligent transportation systems for bridge condition assessment: current status and future direction, IEEE Transactions on Intelligent Transportation Systems 17 (8) (2016) 2107–2122.
[26] B. Peeters, J. Maeck, G. De Roeck, Vibration-based damage detection in civil engineering: excitation sources and temperature effects, Smart materials and Structures 10 (3) (2001) 518.
[27] P. Moser, B. Moaveni, Environmental effects on the identified natural frequencies of the dowling hall footbridge, Mechanical Systems and Signal Processing 25 (7) (2011) 2336–2357.
[28] Y. Yang, J. Yau, Z. Yao, Y. Wu, Vehicle-bridge interaction dynamics: with applications to high-speed railways, World Scientific, 2004.
[29] I. Goodfellow, Y. Bengio, A. Courville, Y. Bengio, Deep learning, Vol. 1, MIT press Cambridge, 2016.
[30] M. Abadi, P. Barham, J. Chen, Z. Chen, A. Davis, J. Dean, M. Devin, S. Ghemawat, G. Irving, M. Isard, M. Kudlur, J. Levenberg, R. Monga, S. Moore, D. G. Murray, B. Steiner, P. Tucker, V. Vasudevan, P. Warden, M. Wicke, Y. Yu, X. Zheng, Tensorflow: A system for large-scale machine learning, in: Proceedings of the 12th USENIX Conference on Operating Systems Design and Implementation, OSDI'16, USENIX Association, Berkeley, CA, USA, 2016, pp. 265–283. URL http://dl.acm.org/citation.cfm?id=3026877.3026899
[31] A. Azizinamini, A new era for short-span bridges, Steel Bridge News (2009) 1–2.
[32] M. Hirt, J.-P. Lebet, Steel bridges: conceptual and structural design of steel and steel-concrete composite bridges, Epfl Press, 2013.
[33] M. A. Grubb, K. E. Wilson, C. D. White, W. N. Nickas, Load and resistance factor design (lrfd) for highway bridge superstructures-reference manual, Tech. rep. (2015).
[34] A. K. Chopra, Dynamics of Structures (2012) 174–196.
[35] K. Huebner, D. Dewhirst, D. Smith, T. Byrom, The finite element method for engineers, John Wiley & Sons, 2008.
[36] A. Kassimali, Matrix Analysis of Structures SI Version, Cengage Learning, 2012.
[37] J. Lundström, Road roughness etimation using available vehicle sensors (2009).

[38] ISO, Mechanical vibration-road surface profiles-reporting of measured data (1995).
[39] M. Agostinacchio, D. Ciampa, S. Olita, The vibrations induced by surface irregularities in road pavements–a matlab® approach, European Transport Research Review 6 (3) (2014) 267–275.
[40] K. Yuen, Bayesian methods for structural dynamics and civil engineering, John Wiley & Sons, 2010.
[41] Y. Xia, H. Hao, G. Zanardo, A. Deeks, Long term vibration monitoring of an rc slab: temperature and humidity effect, Engineering Structures 28 (3) (2006) 441–452.
[42] H. Liu, X. Wang, Y. Jiao, Effect of temperature variation on modal frequency of reinforced concrete slab and beam in cold regions, Shock and Vibration 2016.
[43] J. Reynolds, Thermal stresses and movements in bridges.
[44] A. Deraemaeker, E. Reynders, G. De Roeck, J. Kullaa, Vibration-based structural health monitoring using output-only measurements under changing environment, Mechanical systems and signal processing 22 (1) (2008) 34–56.
[45] I. Behmanesh, B. Moaveni, Accounting for environmental variability, modeling errors, and parameter estimation uncertainties in structural identification, Journal of Sound and Vibration 374 (2016) 92–110.
[46] National centers for environmental information.
URL `https://www.ncdc.noaa.gov/`
[47] J. Tompson, K. Schlachter, P. Sprechmann, K. Perlin, Accelerating eulerian fluid simulation with convolutional networks, arXiv preprint arXiv:1607.03597.
[48] R. Grzeszczuk, D. Terzopoulos, G. Hinton, Neuroanimator: Fast neural network emulation and control of physics-based models, in: Proceedings of the 25th annual conference on Computer graphics and interactive techniques, ACM, 1998, pp. 9–20.
[49] Y. Xu, J. Du, L.-R. Dai, C.-H. Lee, A regression approach to speech enhancement based on deep neural networks, IEEE/ACM Transactions on Audio, Speech and Language Processing (TASLP) 23 (1) (2015) 7–19.
[50] N. Srivastava, G. Hinton, A. Krizhevsky, I. Sutskever, R. Salakhutdinov, Dropout: a simple way to prevent neural networks from overfitting, The Journal of Machine Learning Research 15 (1) (2014) 1929–1958.
[51] S. Zheng, Y. Song, T. Leung, I. Goodfellow, Improving the robustness of deep neural networks via stability training, in: Proceedings of the ieee conference on computer vision and pattern recognition, 2016, pp. 4480–4488.
[52] N. M. Nasrabadi, Pattern recognition and machine learning, Journal of electronic imaging 16 (4) (2007) 049901.
[53] R. Heywood, W. Roberts, G. Boully, Dynamic loading of bridges, Transportation Research Record: Journal of the Transportation Research Board (1770) (2001) 58–66.
[54] G. Palshikar, et al., Simple algorithms for peak detection in time-series, in: Proc. 1st Int. Conf. Advanced Data Analysis, Business Analytics and Intelligence, 2009, pp. 1–13.
[55] S. Hochreiter, J. Schmidhuber, Long short-term memory, Neural computation 9 (8) (1997) 1735–1780.
[56] G. E. Batista, R. C. Prati, M. C. Monard, A study of the behavior of several methods for balancing machine learning training data, ACM SIGKDD explorations newsletter 6 (1) (2004) 20–29.